

Fe impurity induced ion-nanopatterning: atomistic simulations using a new force field for FeSi

P. Süle

*Research Institute for Technical Physics and Material Science,
Konkoly Thege u. 29-33, Budapest, Hungary,
sule@mfa.kfki.hu, www.mfa.kfki.hu/~sule,*

(Dated: February 28, 2024)

The ion-bombardment induced nanopatterning of Si(001) has been simulated by atomistic simulations with and without Fe impurity. The surface contamination has been simulated by using a new force field developed for FeSi. This is a fitted bond order potential (BOP) given for Si and for Fe by Albe et al. This BOP formula has been optimized simultaneously for FeSi, Si and for Fe. Using this new force field we are able to follow the ion-beam assisted deposition for Si in the presence of Fe contamination in the surface region. As an overall result, we get an unexpectedly rich variety of nanopatterns formed by the reorganization of the crater rims of the individual ion impacts. The previously thought simple atomistically roughened surfaces show unprecedented landscapes and topography with nanoscale features. The characteristic size of the units of the pattern is in the range of a few nms. Typical of the occurred pattern is the network of interconnected elongated adatom islands. We also see the self-organization of this pattern upon ion-bombardments. At 50° impact angle we get a nanoporous surface (sponge-like) both for Fe-contaminated and Fe-free simulations. At 70° of impact (grazing angle of incidence) the pattern resembles to that of elongated atomic chains (adatom islands) along the ion impact direction. This latter pattern could be understood as a prepattern state towards rippling. At lower angles (30°) nanoholes rule the landscape. The obtained pattern corresponds to low fluence experiments which are used to consider as simple roughening without showing any sing of patterning.

PACS numbers: 68.35.-p, 79.20.Rf, 81.65.Cf, 61.82.Fk

INTRODUCTION

Self-assembly, that is the spontaneous formation of regular structures, has become a critical implement in the toolbox of nanotechnologists. Self-organising functional nano-systems and nano-devices are the ultimate aim of bottom-up nano-fabrication [1]. The spontaneous organisation can be exploited for nanopatterning (NP) a variety of materials using a variety of nanotechnological tools [1]. Affordable surfaces with well-controlled nanostructures over a large area open new applications not only in electronics but also in the physical world through their unique properties originating from their nanoscale geometry. The direct nanofabrication of the surface (top-down approach) using coupled interference lithography with deep reactive ion etching also become an efficient tool recently for nanofabrication, although, the required number of technological steps could be still too large. [2, 3].

So far much of the work related to self-assembling nanostructures (bottom-up) has been nothing more than demonstrations in university laboratories. Therefore, the building up of regular nanopatterns using the spontaneous formation of surface features remains still an unexplored area of nanoscience in the sense of nanotechnology.

Even at basic research level the tailored and controlled way of surface nanofabrication is still challenging although a great deal of efforts have been done in the last decades towards the understanding of processes responsible for the formation of regular patterns [4, 5, 7].

Ion-sputtering induced self-organized surface nanopatterning is a widely used bottom-up technique for nanofabrication mostly still at a basic research level, however, possible potential application fields such as the mass-fabrication of nanotemplates remains still challenging

[4, 5]. Although the cost-effective self-organized regulation of the nanotopography of nanotemplates is still lacking, the ability of manipulating the surface topography in the nanoscale using a single technological step (or replacing an another top-down step) based on the phenomenon of self-assembly is an important issue and a great challenge in nanoscience.

The self-organization induced formation of dot pattern has already been demonstrated on semiconductors [5]. Periodic ripple formation on surfaces has been the subject of numerous experimental [7] and theoretical works [16, 17]. The formation of ripples on Si has also been reported recently [18, 19]. In general, however, the fundamental understanding of the self-organization of nanoscale periodic surface features is still lacking.

In order to understand the processes which could control self-organized NP an efficient simulation tool is required. The available theoretical and computational (numerical) techniques mostly do not go beyond the level of phenomenology and continuum approaches [20]. Recently, impurity effects have been considered within a continuum model [6]. Using these approaches, however, the atomistic details of NP remain inaccessible.

Atomistic computer simulations based on kinetic Monte Carlo approach have already been used for modelling self-organized nanopatterning [17, 21–23]. Although, molecular dynamics (MD) simulations have yet been employed for following the time evolution of ion-patterning with some success [13, 14], however, simulations starting from a flat surface has not yet been utilized. In the present work we would like to show that upon low-fluence ion-sputtering early-patterning takes place with features similar to that of occur at higher fluences. Prepatterns which can be obtained upon $< 10^{16}$ ion/cm² fluences although show irregular features, the

occurring network of adatom islands could evolve into regular patterns upon higher ion-fluence. Hence in the early stage of NP a random disorder is found which is, however, shows the characteristics of nanoporous Si under certain conditions. The transition of the disordered to ordered topography transition is still unreachable with the available computational techniques.

The key questions to be answered are the followings:
 How to rule the surface topography ?
 Which steps are encountered during the surface height evolution by the topography ?
 How various patterns transform into each other ? What is the atomistic mechanism of self-organization of regular surface features ?

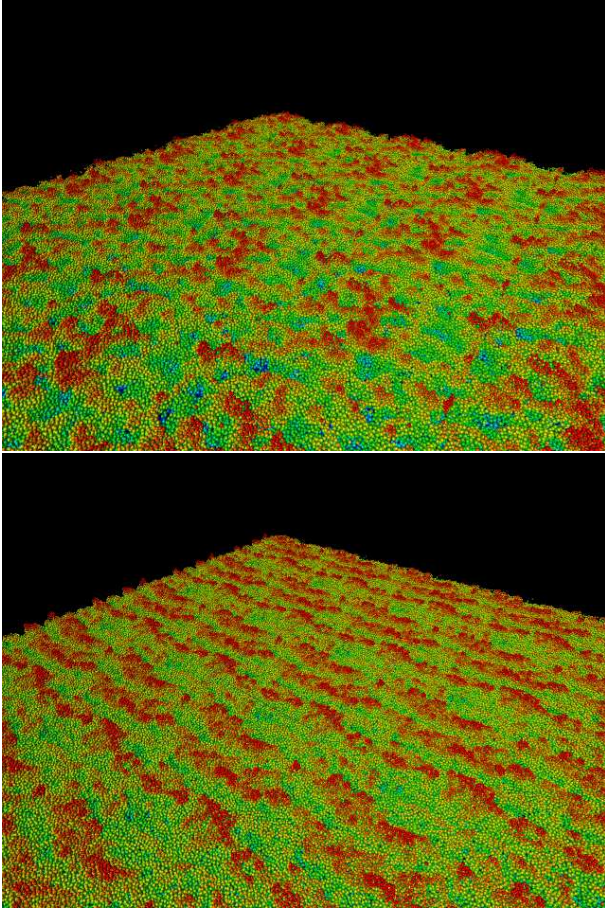


FIG. 1: The color coded topography images of the bombarded surfaces with (ibad, Fig 1a) and without (noibad, Fig 1b) Fe impurities.

THE FITTING OF THE ALBE-ERHART EMPIRICAL POTENTIAL FOR FESI

It is assumed that the energy of a system can be separated into a sum of pairwise contributions V_{ij} ,

$$E = \sum_{ij, i>j} f_{ij}(r_{ij})[V_{ij}^R - b_{ij}V_{ij}^A(r_{ij})], \quad (1)$$

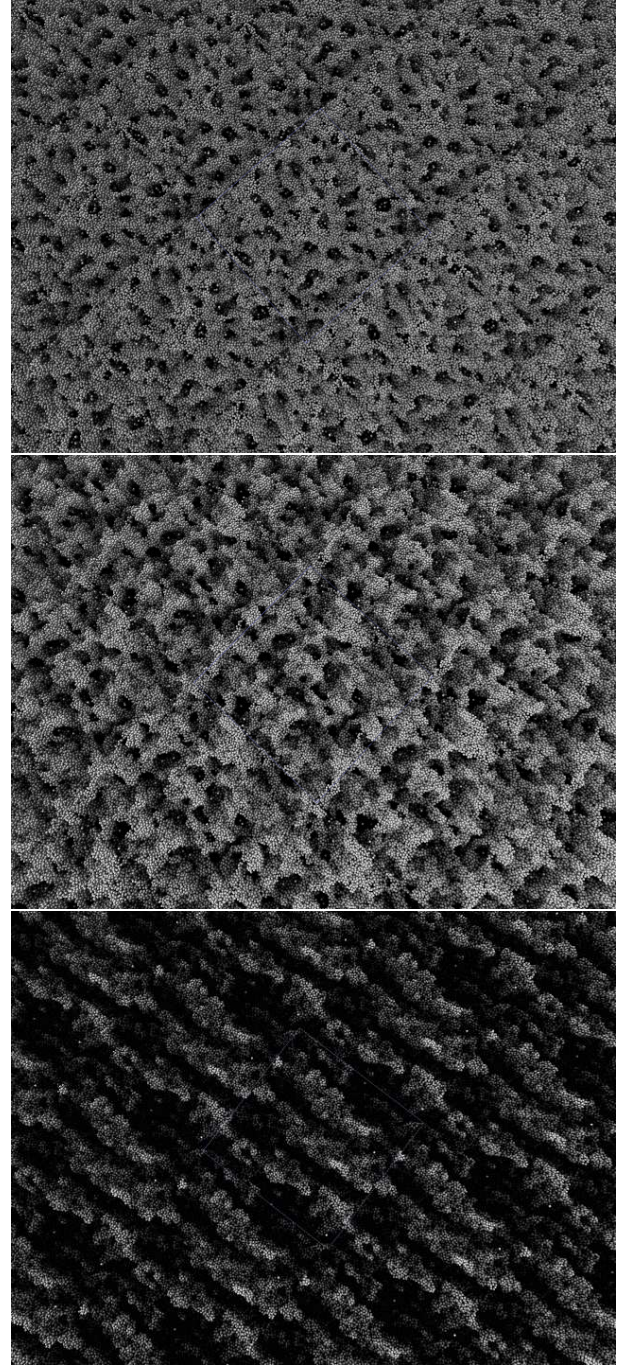


FIG. 2: Color coded (gray) height images of ion-sputtered surfaces of aSi (without Fe impurities, no ibad) at 30° , 50° and 70° using 500 eV Xe^+ impacts (1300 repeated impacts randomly distributed over the whole area). Periodic images of the original simulation cell is shown magnified 3 times (the original cell size was 162 Å) and the present images correspond to roughly $80 \times \sim 80 \text{ nm}^2$ area.

where for the repulsive and attractive pair interactions we have the following formulas :

$$V_{ij}^R = \frac{D_0}{S-1} \exp(-\beta \sqrt{2S}(r-r_0)), \quad (2)$$

$$V_{ij}^A = \frac{SD_0}{S-1} \exp(-\beta \sqrt{2/S}(r-r_0)), \quad (3)$$

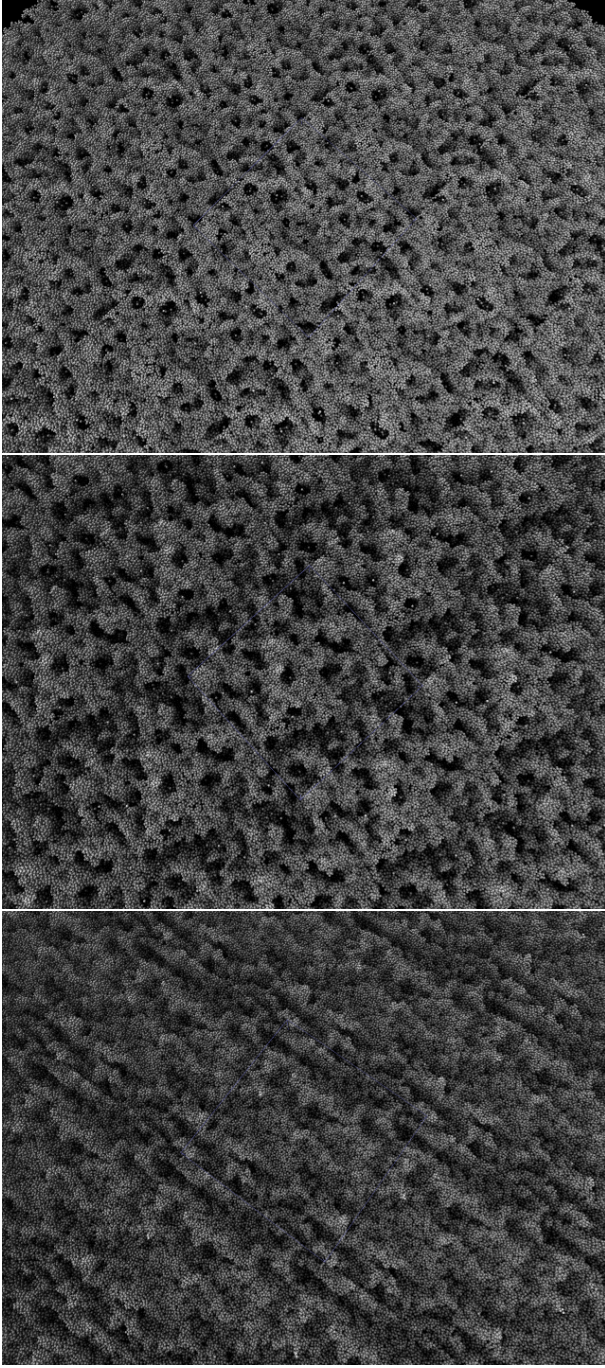


FIG. 3: Color coded (gray) height images of ion-sputtered surfaces of aSi (with Fe impurities, ibad) at 30° , 50° and 70° using 500 eV Xe^+ impacts (1000 repeated impacts randomly distributed over the whole area). Periodic images of the original simulation cell is shown magnified 3 times (the original cell size was 162 Å) and the present images correspond to roughly $80 \times \sim 80 \text{ nm}^2$ area.

respectively.

The bond-order b_{ij} depends on the chemical environment of the atoms i and j. It is given by

$$b_{ij} = (1 + \chi_{ij}^n)^{\frac{1}{2n}} \quad (4)$$

with

$$\chi_{ij} = \sum_{k(\neq i,j)} f_{ik}^c(r_{ik}) g_{ik}(\Theta_{ijk}) \exp[2\mu_{ik}(r_{ij} - r_{ik})] \quad (5)$$

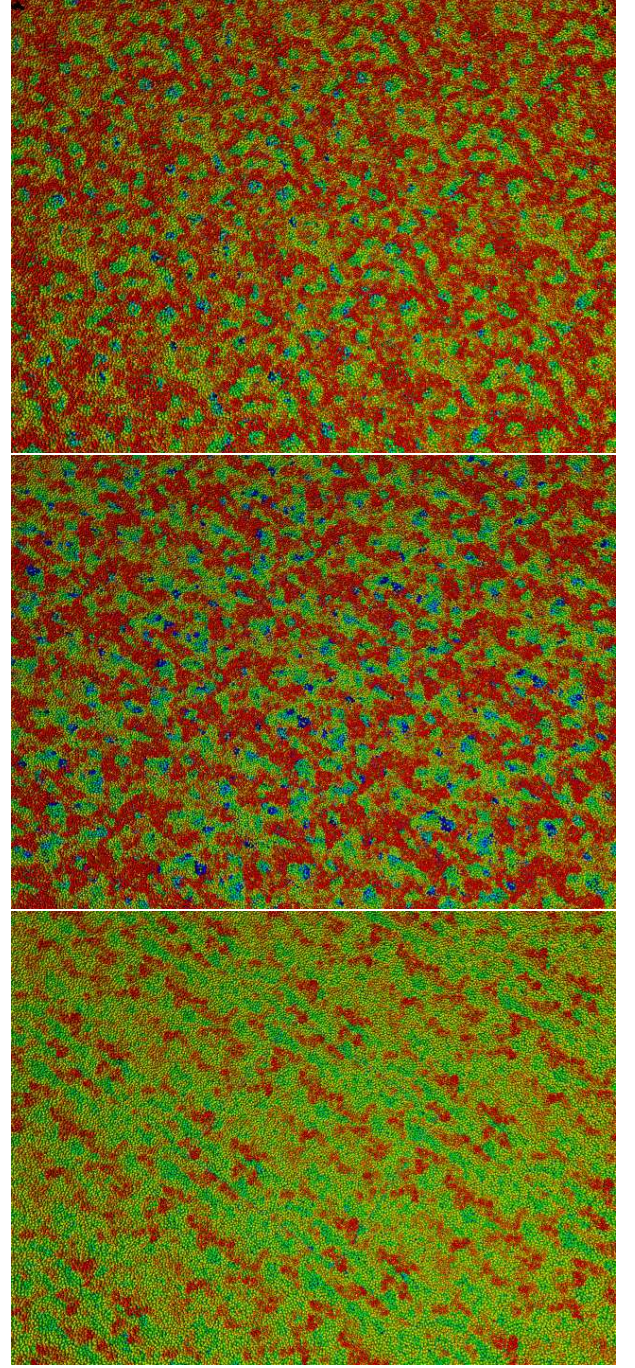


FIG. 4: Color coded (rainbow) height images of ion-sputtered surfaces of aSi (with Fe impurities, ibad) at 30° , 50° and 70° using 500 eV Xe^+ impacts (1000 repeated impacts randomly distributed over the whole area). Periodic images of the original simulation cell is shown magnified 3 times (the original cell size was 162 Å) and the present images correspond to roughly $80 \times \sim 80 \text{ nm}^2$ area.

and where the angular term $g(\Theta)$,

$$g(\Theta) = \gamma \left(1 + \frac{c^2}{d^2} - \frac{c^2}{d^2 + (h + \cos\Theta)^2} \right). \quad (6)$$

By construction, the BOP potential includes only nearest neighbor interactions. This necessitates the use of a cutoff function $f_{ij}(r)$, which scales the energy between the first and second neighbors shells smoothly to zero.

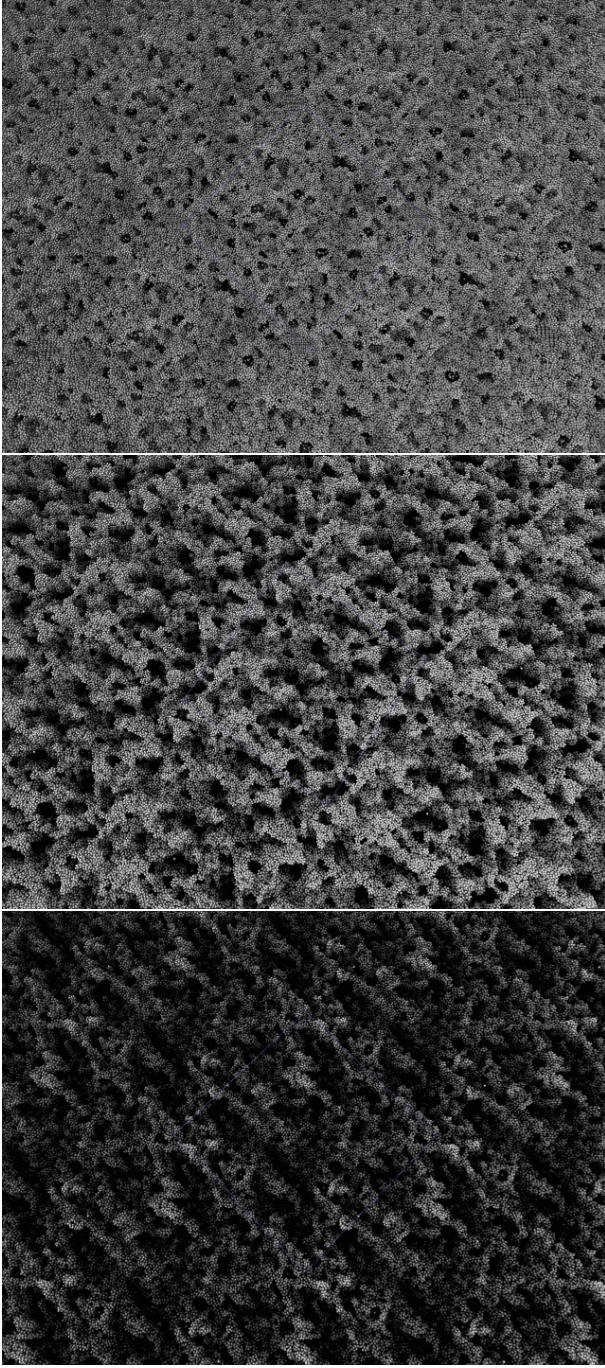


FIG. 5: Color coded (gray) height images of ion-sputtered surfaces of Si(001) codeposited with Fe (ibad) 30°, 50° and 70° using 500 eV Kr^+ impacts (1000 repeated impacts randomly distributed over the whole area).

The cutoff function is

$$f_{ij}(r_{ij}) = \begin{cases} 1 & r \leq R_c - D_c \\ \frac{1}{2} - \frac{1}{2} \sin[\frac{\pi}{2}(r - R_c)/D_c] & |r - R_c| \leq D_c \\ 0 & r \geq R_c + D_c \end{cases}$$

where R_c Å is the cutoff distance and D_c Å is the damping distance.

The BOP potential has been parametrized using an extended training set of various structures (B1 (NaCl), B2 (CsCl), B3 (ZnS) and B20 (eps-FeSi) phases for FeSi).

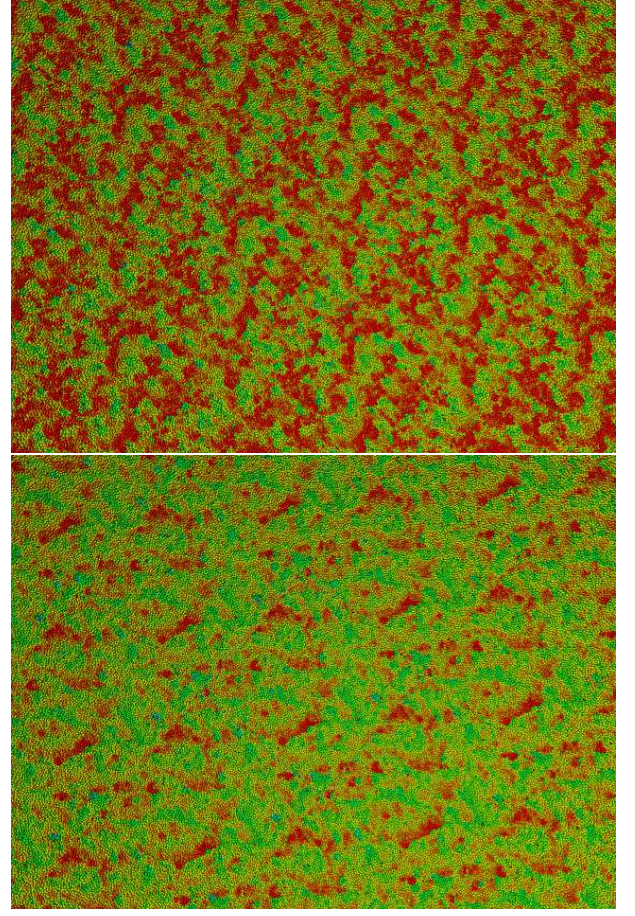


FIG. 6: Color coded (gray) height images of ion-sputtered surfaces of FeSi without and with Fe codeposition (Fig 1a and 1b) at 50° 500 eV Xe^+ impacts (1000 repeated impacts randomly distributed over the whole area).

The parametrization procedure has been carried out using the PONTIFIX code developed by P. Erhart [9]. The parameters of FeSi have simultaneously been fitted together with the elemental Si and Fe parameters. For the elements similar data base has been used given by Albe and Erhart [9]. *ab initio* SIESTA [11] calculations were used to determined the cohesive energies of various structures. A Levenberg-Marquardt least-squares algorithm [12] has been implemented in Pontifix to find a combination of parameters which minimizes the deviation between the properties in the fitting database and the properties predicted by the potential. Parameter sets for different interaction types can be fitted simultaneously. The fitting database encompassed the bond lengths and energies of various structures as well as elastic constants.

THE SETUP OF THE SIMULATION

Classical constant volume molecular dynamics simulations were used to simulate the ion-solid interaction using the PARCAS code [30] and a shell script code written in our laboratory for simulating ion-sputtering using an atomic serial addition procedure [14]. Further details are given in recent communications [14, 29]. The Tersoff potential has been used for Si together with a ZBL

TABLE I: The fitted parameters used in the bond order interatomic potential for Fe-Si, Fe-Fe and for Si-Si.

| | Fe-Si | Fe-Fe | Si-Si |
|----------------------------|-----------|----------|----------|
| D_0 (eV) | 4.635031 | 2.877707 | 3.761432 |
| r_0 (Å) | 1.546801 | 1.595041 | 2.170624 |
| S | 2.330520 | 8.385355 | 1.536018 |
| β (Å ⁻¹) | 1.058204 | 1.127692 | 1.285636 |
| γ | 0.078319 | 0.026045 | 0.099010 |
| c | 0.403341 | 1.481643 | 0.350297 |
| d | 0.197786 | 0.234050 | 0.280854 |
| h | -0.181581 | 0.263854 | 0.220250 |
| n | 0.782953 | 5.417789 | 0.955404 |
| 2μ | 0.0 | 0.0 | 0.0 |
| R_c (Å) | 2.983063 | 2.444649 | 3.299024 |
| D_c (Å) | 0.2 | 0.2 | 0.15 |

^a

TABLE II: The test of the preformance of the BOP potential with the new parameter set

| | present work | experimental |
|---------------------------|----------------|--------------|
| FeSi (B20) | | |
| lattice constant (Å) | 4.52 | 4.49 |
| melting point (K) | 1600 ± 100 | 1550 |
| cohesive energy (eV/atom) | 4.89 | 4.87 |
| surface energy (eV/atom) | 0.59 | 0.8 |
| bulk modulus (GPa) | 185. | 160. |
| Fe | | |
| lattice constant (Å) | 2.83 | 2.87 |
| melting point (K) | 1900 ± 50 | 1810 |
| cohesive energy (eV/atom) | 4.31 | 4.28 |
| surface energy (eV/atom) | | |
| bulk modulus (GPa) | 129 | 169 |
| B' | 3.1 | 5.1 |
| Si | | |
| lattice constant (Å) | 5.43 | 5.43 |
| melting point (K) | 1730 ± 50 | 1687 |
| cohesive energy (eV/atom) | 4.63 | 4.63 |
| surface energy (eV/atom) | 0.8-1.7 | 1.2 |
| bulk modulus (GPa) | 102 | 99 |

like repulsive potential which smoothly joined together [32]. Comparative studies on the crater formation on Si showed the reasonable performance for this potential [31]. A Tersoff-type crosspotentials Xe-Si, Xe-Fe, Kr-Si, Kr-Fe, have been fitted to *ab initio* calculations [33]. The details of such a fitting process is given elsewhere [14]. The profiles of the fitted potentials are shown in Fig. 6.

The parameters for the fitted pair-potentials are given in Table III.

The emerging excess heat has been controlled by the Berendsen heat bath at the bottom of the cells. We irradiate the surface of Si(110) in an initially diamond crystal structure with different length.

We employ our recently developed computer code for handling conditions appear during simulated ion-sputtering [14]. This code has also seriously been developed and adapted for this particular problem. Repeated ion impacts with 0.5 keV Xe⁺ ions are initialized with a time interval of 0.5-5 ps between each of the ion-impacts. The initial velocity direction of the impacting atom was 30°, 50° and 70° with respect to the surface

TABLE III: The fitted semiempirical parameters used in the Tersoff interatomic potential for Xe-Si Kr-Si, Xe-Xe and for Kr-Kr.

| | A | B | λ | μ |
|-------|----------|----------|-----------|---------|
| Xe-Si | 163.123 | -3291.89 | 125.676 | 3.11012 |
| Xe-Xe | 6000.8d0 | 95.2 | 2.47990 | 1.7322 |
| Kr-Si | 3723.32 | -750.317 | 5.17001 | 2.94665 |
| Kr-Kr | 1082.06 | -715.546 | 2.84947 | 2.85043 |

^aNote, that the rest of the parameters of the Tersoff formalism have not been used which occur in the bond-angle dependent part by setting $\beta = 0$. [32]. The Tersoff parameters can be converted into the parameters of the BOP formalism. Hereby we use the parameters of the original radial part of the Tersoff potential and which has been fitted to *ab initio* calculations [14].

normal. We randomly varied the impact position. In order to approach the real sputtering limit a large number of ion irradiation are employed using automated simulations conducted subsequently together with analyzing the history files (movie files) in each irradiation steps. In this article we present results up to 1000 ion irradiation which we find suitable for comparing with low to medium fluence experiments. 1000 ions are randomly distributed over a $\sim \lambda \times 54 \text{ Å}^2$ area which corresponds to $< 10^{15}$ ion/cm² ion fluence.

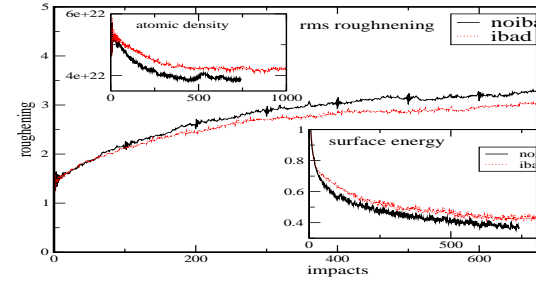


FIG. 7: The evolution of the surface energy (eV/atom) and rms surface roughening (Inset) as a function of the Xe⁺ ion impacts at 500 eV and 30° incidence angle for iob-beam assisted deposition and without Fe impurities.

In order to avoid artificial effects in the topography, such as overheating induced border walls of particles, the temperature has been softly quenched to 300 K after 2.5 ps at each ion-impact steps using temperature controll at the borders. Although this way of temperature controll seems to be efficient, one has to keep in mind that radiation enhanced thermal diffusion has been excluded in our computer experiments. Ballistic dissusion and thermal spike (TS) is still accounted for in this modell since collisional cascades and the subsequent heat spike terminates within few ps [26]. Hence it is reasonable to apply an artificial quenching process right after the TS to avoid the overheating of the cell. It is also known from simulations that repeated ion-impacts induce damage accumulation which stimulates partly radiation enhanced

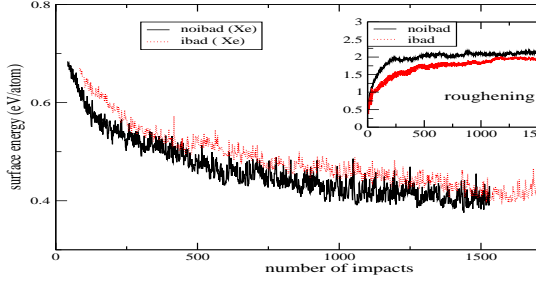


FIG. 8: The evolution of the surface energy (eV/atom) and rms surface roughening (Inset) as a function of the Xe^+ ion impacts at 500 eV and 50° incidence angle for iob-beam assisted deposition and without Fe impurities.

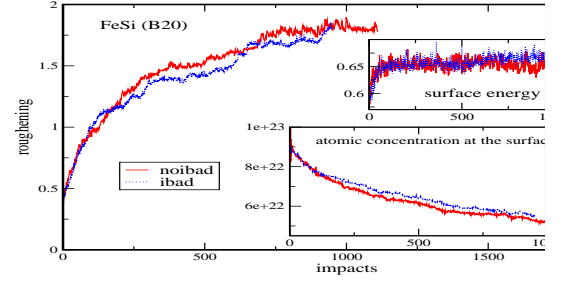


FIG. 10: The evolution of rms surface roughening, surface energy (eV/atom) and atomic concentration at the roughening surface are shown as a function of the 500 eV Xe^+ ion impacts and at 50° incidence angle for iob-beam assisted deposition (ibad) and without Fe impurities (noibad) for the B20 phase of FeSi.

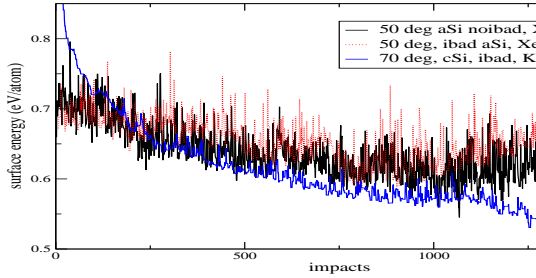


FIG. 9: The evolution of the surface energy (eV/atom) as a function of the Xe^+ ion impacts at 500 eV and 50° and 70° incidence angle for iob-beam assisted deposition and without Fe impurities on aSi and cSi flat surfaces.

diffusion (RED) [26]. RED goes on a longer time scale than TS. Its medium time scale range (from few ps up to a ns) could be followed within our model at 300 K.

It has also been concluded in our recent paper [14] that it is unlikely that thermal motion on a much longer time scale is responsible for ion-induced nanopatterning and only minor smoothing effects on the topography could be accounted for thermal diffusion. Instead we emphasize that ballistic diffusion is responsible for NP. We expect such ballistic motion of "hot" particles terminate within 2.5 ps.

This work is supported by the OTKA grant K-68312 from the Hungarian Academy of Sciences. Support from the bilateral German-Hungarian exchange program DAAD-MÖB (Grant No. 37-3/2008) and German Science Foundation (DFG research group 845, project HE2137/4-1) is also acknowledged. We wish to thank to K. Nordlund for helpful discussions and constant help. The work has been performed partly under the project

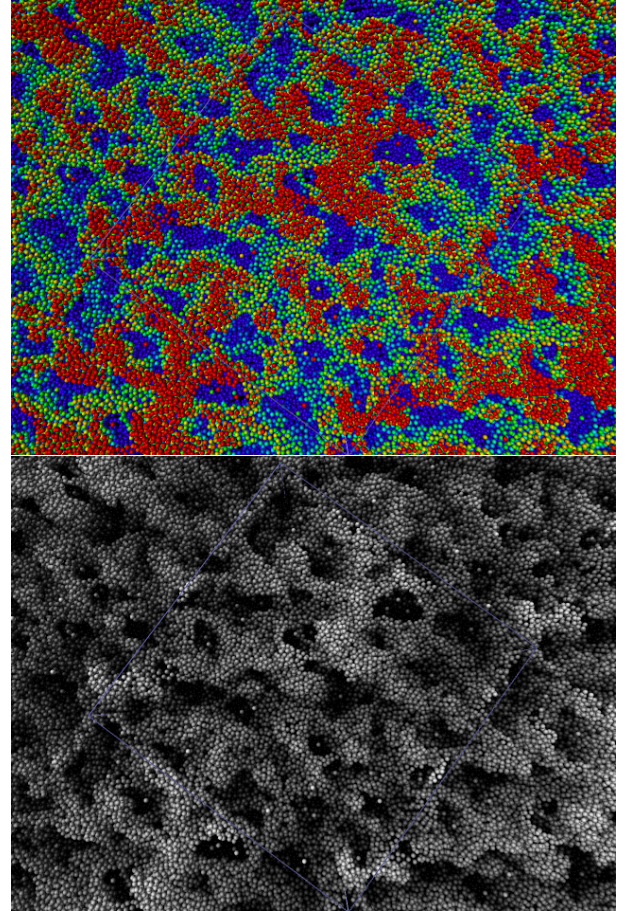


FIG. 11: Color coded (rainbow and gray) height images of ion-sputtered surfaces of aSi (noibad) at 50° 500 eV Xe^+ impacts. The scanned area is $22.3 \times 22.3 \text{ nm}^2$. (2000 repeated impacts randomly distributed over the whole area).

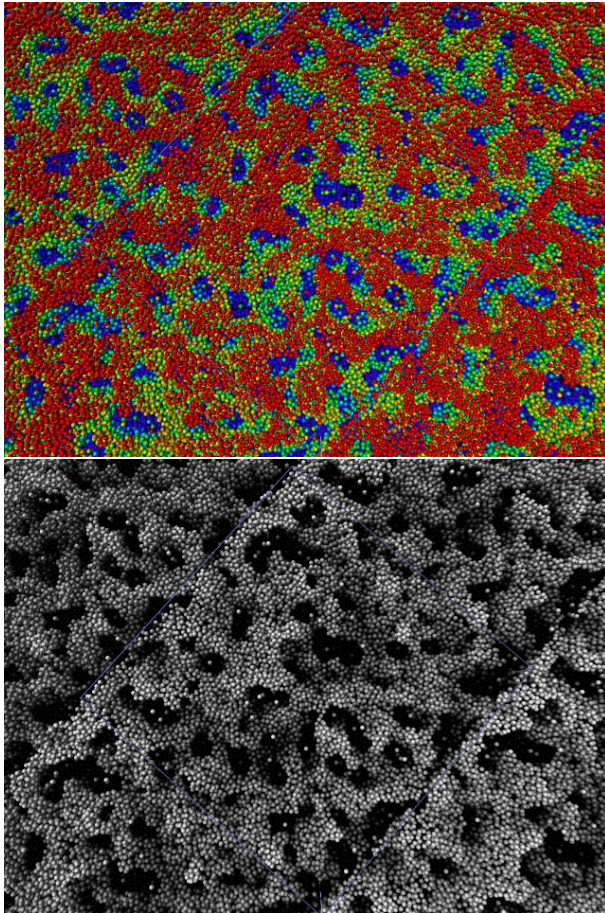


FIG. 12: Color coded (rainbow and gray) height images of ion-sputtered surfaces of aSi (noibad) at 30° 500 eV Xe^+ impacts. The scanned area is 20×20 nm². (2000 repeated impacts randomly distributed over the whole area).

HPC-EUROPA with the support of the European Community using the supercomputing facility at CSC in Espoo.

-
- [1] L. Tapasztó, G. Dobrik, P. Lambin, L. P. Biro, *Nature Nanotechnology*, **3** 397. (2008).
 - [2] C-H. Choi and C.-J. Kim, *Phys. Rev. Lett.* **96**, 066001 (2006).
 - [3] F. Huo, G. Zheng, X. Liao, L. R. Giam, J. Chai, X. Chen, W. Shim, C. A. Mirkin, *Nature Nanotechnology*, **5**, 637 (2010).
 - [4] J. Li, D. Stein, C. McMullan, D. Branton, M. J. Aziz and Jene A. Golovchenko, *Nature* **412**, 166. (2001).
 - [5] S. Facsko, T. Dekorsy, C. Koerdts, C. Trappe, H. Kurz, A. Vogt, and H. L. Hartnagel, *Science* **285** 1551. (1999).
 - [6] J. Zhou, M. Lu, *Phys. Rev.* **B82**, 125404(2010).
 - [7] U. Valbusa, C. Boragno, F. Buatier de Mongeot, *J. Phys. Cond. Matt.* **14**, 8153 (2002).
 - [8] S. Macko, F. Frost, B. Ziberi, D. F. Forster, and T. Michely, *Nanotechnology* **21**, 085301 (2010).
 - [9] M. Müller, P. Erhart and K. Albe, *J. Phys.: Condens. Matter* **19**, 326220 (2007), P. Erhart and K. Albe, *Phys. Rev.* **B71**, 035211 (2005).
 - [10] A. Stukowski, *Modell. and Simul. in Mater. Sci. and Eng.*, **18**, 015012 (2010).
 - [11] E. Artacho, E. Anglada, O. Dieguez, J. D. Gale, A. Garca, J. Junquera, R. M. Martin, P. Ordejón, J. M. Pruneda, D. Sánchez-Portal and J. M. Soler, *J. Phys.: Condens. Matter* **20**, 064208 (2008).
 - [12] Press, W. H., S. A. Teukolsky, W. T. Vetterling, and B. P. Flannery, 1995, *Numerical Recipes in Fortran 77: The Art of Scientific Computing* (Cambridge University Press, New York), chapter 11, 2nd edition.
 - [13] P. Süle, *J. Chem. Phys.*, **134**, 244706 (2011).
 - [14] P. Süle and K.-H. Heinig, *J. Chem. Phys.* **131**, 204704 (2009).
 - [15] P. Süle, *Nucl. Inst. and Methods in Physics Research*, **B268**, 1404 (2010).
 - [16] M. A. Makeev, R. Cuerno, A. L. Barabasi, *Nucl. Instrum. Meth. in Phys. Res.* **B197**, 185 (2002).
 - [17] W. L. Chan, E. Chason, *J. Appl. Phys.* **101**, 121301-1 (2007).
 - [18] J. Erlebacher, M. J. Aziz, E. Chason, M. B. Sinclair, and J. A. Floro, *Phys. Rev. Lett.* **82**, 2330 (1999), B. Ziberi, F. Frost, Th. Höche and B. Rauschenbach *Phys. Rev.* **B72**, 235310 (2005). *Appl. Phys. Lett.* **92**, 063102 (2008).
 - [19] A. Keller, R. Cuerno, S. Facsko, and W. Möller, *Phys. Rev.* **B79**, 115437 (2009).
 - [20] L. Rontzsch, K.-H. Heinig, J. A. Schuller, M. L. Brongersma, L. Mark, *Appl. Phys. Lett.* **90**, 044105 (2007).
 - [21] M. Stepanova and S. K. Dew *Appl. Phys. Lett.* **84** 1374 (2004).
 - [22] E. O. Yewanda, R. Kree, and A. Hartmann, *Phys. Rev.* **B75**, 155325 (2007).
 - [23] M. Strobel, K.-H. Heinig, T. Michely, *Surf. Sci.*, **486**, 136 (2001).
 - [24] M. Moseler, P. Gumbsch, C. Casiraghi, A. C. Ferrari, J. Robertson, *Science* **309**, 1545 (2005).
 - [25] N. Kalyanasundaram, M. Ghazisaeidi, J. B. Freund, *et al.*, *Appl. Phys. Lett.* **92**, 131909 (2008).
 - [26] P. Süle, M. Menyhárd, K. Nordlund, *Nucl. Instr. and Meth. in Phys. Res.*, **B222**, 525 (2004).
 - [27] W. W. Mullins, *J. Appl. Phys.* **28**, 333 (1957), *J. Appl. Phys.* **30**, 77 (1959).
 - [28] P. Süle *J. Chem. Phys.* **129**, 084707 (2008).
 - [29] P. Süle, M. Menyhárd, L. Kótiš, J. Lábár, W. F. Egelhoff Jr., *J. Appl. Phys.*, **101**, 043502 (2007).
 - [30] K. Nordlund, *Comput. Mater. Sci.*, **3**, 448. (1995).
 - [31] J. Samela, K. Nordlund, J. Keinonen, V.N. Popok, *Nucl. Instr. and Meth. in Phys. Res.* **B255**, 253 (2007).
 - [32] J. Tersoff, *Phys. Rev.* **B37**, 6991. (1988).
 - [33] M. J. Frisch, G. W. Trucks, H. B. Schlegel, *et al.*, Gaussian, Inc., Pittsburgh PA, (2003), see also at: <http://www.gaussian.com>.
 - [34] A. Pimpinelli, J. Villain, *Physics of Crystal Growth*, Cambridge, Univ. Press (1998).
 - [35] W. Eckstein, *Computer Simulation of Ion-Solid Interactions*, (Springer, Berlin 1991).
 - [36] E. Chason, W. L. Chan, and M. S. Bharathi, *Phys. Rev.* **B74**, 224103 (2006).
 - [37] C. Battaglia, K. Gaál-Nagy, C. Monney, C. Didiot, E. F. Schwier, *Phys. Rev. Lett.* **102**, 066102 (2009).